Journal of Zhejiang University-SCIENCE A (Applied Physics & Engineering)
ISSN 1673-565X (Print); ISSN 1862-1775 (Online)
www.zju.edu.cn/jzus; www.springerlink.com
E-mail: jzus@zju.edu.cn

A growth-based topology optimizer for stiffness design of continuum structures under harmonic force excitation*

Bao-tong LI†, Su-na YAN, Jun HONG†‡

(*The State Key Laboratory for Manufacturing Systems Engineering, School of Mechanical Engineering, Xi'an Jiaotong University, Xi'an 710049, China*)

†E-mail: baotong.me@mail.xjtu.edu.cn; jhong_email@163.com

Received Dec. 7, 2015; Revision accepted Apr. 18, 2016; Crosschecked Nov. 11, 2016

Abstract: The aim of this study is to explore the potential of various plant ramifications as concept generators for creating a brand topology optimization solution for stiffness design of continuum structures under harmonic force excitations. Firstly, a mathematical model is built to identify analytical laws that underlie the optimality of the effective but individual design rules of existing leaf venation morphogenesis. Then, a new evolutionary algorithm is developed to find the optimal topology of stiffened structures under harmonic force excitations. Candidate stiffeners are treated as being alive, growing at locations with a maximum displacement response gradient along the structural surface. Since the scale of the candidate stiffeners can be adaptively expanded or reduced during the simulation, computational resources could be saved, thereby enhancing the flexibility of topology optimization. Finally, the suggested approach is applied to a case study in which the displacement amplitude at specified locations is defined as the objective and the volume of added stiffeners as the constraint. The simulation process shows how the stiffness design of continuum structures can be conducted automatically using this bionic approach.

Key words: Topology optimization, Adaptive growth, Stiffness design, Stiffener layout, Harmonic force excitation
http://dx.doi.org/10.1631/jzus.A1500328 **CLC number:** TH11

1 Introduction

Vibration is inevitable in working mechanical structures and has distinctly negative effect on their performances, which raises the issue of structural vibration control. Common approaches to vibration control usually involve developed structures, applying passively or actively controlled friction dampers (Gaul and Becker, 2014; Zhang *et al*., 2014) or changing the working parameters of machines (Meehan, 2002; Bhogal *et al*., 2015). Some studies have focused on reliability computation (Viadero *et al*., 1994) and chatter reliability prediction of mechanical systems by taking the uncertainty of system parameters into account (Graham *et al*., 2013; Liu *et al*., 2016). However, in such approaches, the material of the mechanical structures is not fully exploited for reducing the dynamic response of structures. At a more fundamental level, the dynamic performance could be taken into account at a very early stage of the development of mechanical structures, namely the structural design stage.

An alternative approach for structural dynamic performance design is to improve structural natural frequencies (Senba *et al*., 2013; Rashid *et al*., 2014; Wetherhold and Padliya, 2014) so that the excitation frequency can be avoided and the structural dynamic response can be indirectly reduced. However, in practical engineering environments, there is always more than one excitation source with different

‡ Corresponding author

* Project supported by the National Natural Science Foundation of China (No. 51405377), the National Science and Technology Major Project of China (No. 2015ZX04014021), and the Fundamental Research Funds for the Central Universities of China (No. xjj2014017)

ORCID: Bao-tong LI, http://orcid.org/0000-0002-8935-0378; Jun HONG, http://orcid.org/0000-0002-0724-3422

excitation frequencies, and it is usually difficult to avoid all the excitation frequencies. On the other hand, design approaches aiming to decrease directly the structural response are much more straightforward and have drawn the attention of researchers. Palmer and Paez (2011) studied the peak response probability distribution of optics under the random excitation of the housing, which could provide guidance for the design of optomechanical sub-assemblies. Li *et al*. (2011) used the Riccati transfer matrix method to develop a dynamic model to predict the natural frequencies and structural responses of large-scale rotary machines subject to axial excitation. By considering the displacement and acceleration responses, Li *et al*. (2013) studied the effectiveness of the market-based control (MBC) strategy for vibration control of a large-scale engineering structure.

Stiffened shell/plate structures are widely used in mechanical structures because of their advantage in improving structural static and dynamic performance with low material consumption. The layout of stiffeners greatly influences structural mechanical performance. In various structural design methods, topology optimization is featured by allowing for increasingly efficient designs with a minimal priori knowledge about the structural configuration. A kind of widely used topology optimization method for stiffened shell/plate structure design is continuum topology optimization. With this method, holes or voids are introduced into the continuum structure to find the optimal material distribution. By utilizing the polynomial interpolation scheme (PIS), Liu *et al*. (2013; 2015) proposed an efficient topology optimization method to minimize the displacement response for structures subjected to low- and high-frequency harmonic excitations. Tsai and Cheng (2013) proposed a topology optimization technique to design a structure with maximal fundamental eigenfrequency and desired eigenmode shapes by using the solid isotropic method with penalization (SIMP) method.

Although continuum topology optimization approaches can provide reasonable structural topology for reference by designers, most have the drawbacks of a huge number of design variables and a vague material distribution result. Additional post-processing has to be performed to distinguish the stiffener layout from the vague material distribution. Apart from the additional computation cost, the structural mechanical performance would be reduced due to the elimination of key structural features if the post-processing is not performed appropriately (Zhou and Rozvany, 1991; Haber *et al*., 1996).

As we rack our brains to overcome the above obstacles in stiffener layout design with topology optimization, nature may provide us with some ideas as it has done in other disciplines (Benz *et al*., 2012; Li *et al*., 2012; Díaz-Tena *et al*., 2014). Branching configurations are a very common kind of structural pattern in both the biological and non-biological worlds, and are usually formed through a gradual growth process adaptive to the surrounding environment. Among various branching configurations in nature, leaf venation of plants could be the most similar to the stiffeners of mechanical structures in both structural and functional aspects. When considered from a mechanics viewpoint, leaf venation and stiffeners are both embedded into a base plate to strengthen it to bear dynamic load while consuming as little material as possible. Both leaf venation and stiffeners have distinct layout patterns. By mimicking the configuration of plant leaf venation, Liu *et al*. (2009) proposed an adaptive structural design method for a blade working in a random wind field. By simulating the branching systems in nature, Ding and Yamazaki (2004) developed a simple growth technique for stiffener layout design by modifying the well-known ground structure method, which has been applied successfully in both static and dynamic scenarios. Such a growth-based concept was later extended by the authors (Li *et al*., 2013a; 2013b) to solve minimum compliance problems under single and multi-loading conditions. The literature on bio-inspired topology optimization and the technologies that underpin it are growing fast. However, design problems related to dynamic responses have been relatively less well addressed than those related to fundamental frequencies in spite of their potential significance. The work described in this paper was a natural expansion of the authors' previous work, from static to more complex dynamic scenarios. The mathematical model is further developed to cater for stiffener layout design aiming for optimal structural dynamic displacement response at low material expense. The simulation algorithm is also planned more elaborately in terms of the growth competition

step that is decoupled into two sub-steps: competition for growth orientation and then competition for growth volume. As a consequence, growth material in each growth iteration is fully utilized and allocated only to the most suitable growth orientations, which more closely resembles the growth of leaf venation in nature. Possible applications of the proposed approach could be the vibration-proof design of stiffened structures in machine tools (Whalley *et al*., 2011), rib layout of flexible thin walls (Herranz *et al*., 2005; Campa *et al*., 2011), or cable structures in engineering structures (Li *et al*., 2013).

The excitation force of most mechanical structures can be simplified as a cyclic force which can be converted into the superimposition of multiple harmonic forces through Fourier expansion. Therefore, the impact factors of structural displacement response under harmonic force are analyzed first to identify which factors should be considered in stiffener layout design. Then, a mathematical growth model is built and the criterion for optimal growth is developed. Based on this, an algorithm is developed for the adaptive growth of stiffeners under harmonic force. Finally, numerical examples are described to validate the effectiveness of the approach proposed in this study.

2 Structural displacement response under harmonic excitation

The dynamic load of mechanical structures can be expressed as the superimposition of multiple harmonic forces through Fourier series. Therefore, a harmonic force is adopted to evaluate the influences of an exciting force on structural displacement response. A model in the shape of a willow leaf is selected as the analysis object. The amplitude, direction, acting position, and frequency of a harmonic force can be considered as key elements of the force. To study the influence of these four elements, modal analysis and dynamic analysis of a leaf model are first conducted. The material of the leaf model is assumed to be isotropic, with an elastic modulus of 5.4 MPa, Poisson's ratio of 0.33, and a density of 1800 kg/m^3. Omitting leaf venation, the willow leaf model can be simplified as a thin plate and discretized by shell elements. In both modal analysis and dynamic analysis, all the degrees of freedom (DOFs) of the lower end of the model are constrained to simulate the function of the leaf petiole. The two order modal shapes of the leaf model are shown in Fig. 1. The first order modal shape is the *z*-directional swing movement of the leaf with a natural frequency of 0.27898 Hz. The fourth order modal shape is the *x*-directional swing movement of the leaf with a natural frequency of 4.3819 Hz.

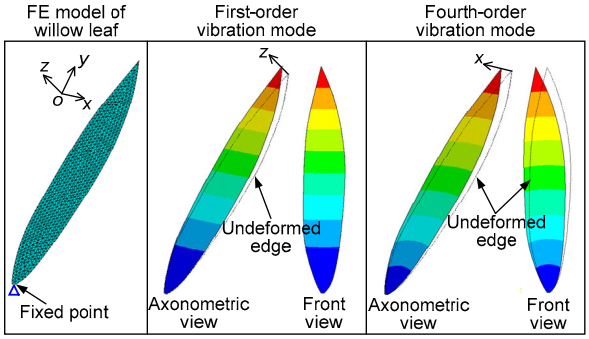

Fig. 1 Finite element (FE) model and modal shapes of the leaf model

In the dynamic analyses, a set of harmonic forces $f(t)=9\cos(2\pi ft)\times10^{-7}$ N are applied to the upper free end of the leaf model with the excitation frequency f changing from 0 to 10 Hz. The forces are applied along the vertical and horizontal directions, respectively. The amplitudes of the displacement responses in the DOF where the harmonic forces are applied are shown in Fig. 2.

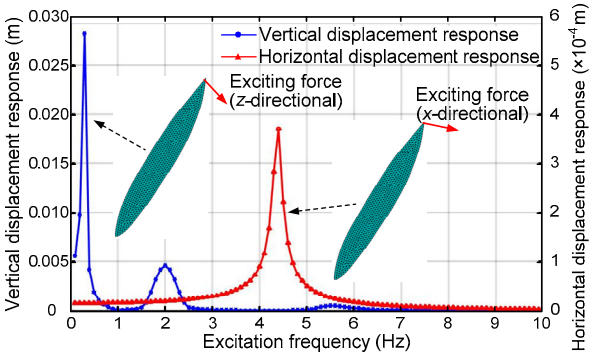

Fig. 2 Displacement response amplitudes under the *x*- or *z*-directional excitation

For a leaf bearing a vertical force, the displacement response amplitude peaks at an excitation frequency of about 0.25 Hz, close to the first order

natural frequency of the leaf, while for a horizontal force, the amplitude peaks at a frequency close to the fourth order natural frequency. Therefore, both the frequency and direction of the exciting force should be taken into account when formulating the mathematical model directing the growth simulation. To study the influence of the four key elements of the exciting force quantitatively, the displacement response of the leaf model is formulated through mode analysis method. The FE leaf model can be considered as a multi-DOF system, whose differential equations of motion under a harmonic exciting force are coupled with each other and can be expressed as

$$\boldsymbol{M}\ddot{\boldsymbol{x}}(t)+\boldsymbol{C}\dot{\boldsymbol{x}}(t)+\boldsymbol{K}\boldsymbol{x}(t)=\boldsymbol{f}(t), \tag{1}$$

where $\boldsymbol{M}$ represents the mass matrix, $\boldsymbol{C}$ represents the damping matrix, $\boldsymbol{K}$ represents the stiffness matrix, $\boldsymbol{f}(t)=\boldsymbol{F}_{\mathrm{A}}\cos(\omega^{*}t)$ is the vector of the exciting force, whose angular frequency is ω^{*} and amplitude vector is $\boldsymbol{F}_{\mathrm{A}}$, and $\boldsymbol{x}(t)$ is the vector of the structural displacement response.

The displacement vectors satisfying Eq. (1) usually consist of two parts: the transient response and the steady-state response. As the steady-state response is caused by the exciting force and the transient response would diminish to zero with time due to damping, only the steady-state displacement response is considered when solving Eq. (1) and conducting the stiffener layout design.

The motion differential equation of the free vibration of the leaf model without damping is

$$\boldsymbol{M}\ddot{\boldsymbol{x}}(t)+\boldsymbol{K}\boldsymbol{x}(t)=\boldsymbol{0}. \tag{2}$$

The characteristic equation of the free vibration leaf without damping is

$$(\boldsymbol{K}-\boldsymbol{\omega}^{2}\boldsymbol{M})\boldsymbol{\Phi}=\boldsymbol{0}, \tag{3}$$

where $\boldsymbol{\Phi}=[\boldsymbol{\varphi}_1, \boldsymbol{\varphi}_2, \ldots, \boldsymbol{\varphi}_n]$ is the modal matrix, $\boldsymbol{\varphi}_i$ is the ith order mode shape, n is the number of structural DOFs, and $\boldsymbol{\omega}=[\omega_1, \omega_2, \ldots, \omega_n]$ is the vector of the natural angular frequency of the leaf model.

As the material of the leaf model is supposed to be isotropic, according to the mode analysis method, the displacement response can be expressed as

$$\boldsymbol{x}(t)=\boldsymbol{\Psi}\boldsymbol{\xi}(t), \tag{4}$$

where $\boldsymbol{\Psi}=[\boldsymbol{\psi}_1, \boldsymbol{\psi}_2, \ldots, \boldsymbol{\psi}_n]$ is the matrix of the regular modal, $\boldsymbol{\psi}_s=\boldsymbol{\varphi}_s\Big/\sqrt{\boldsymbol{\varphi}_s^{\mathrm{T}}\boldsymbol{M}\boldsymbol{\varphi}_s}$ is the sth order regular mode shape, and $\boldsymbol{\xi}(t)$ is the vector of the modal coordinate.

Therefore, the matrix of the regular modal also satisfies

$$(\boldsymbol{K}-\boldsymbol{\omega}^{2}\boldsymbol{M})\boldsymbol{\Psi}=\boldsymbol{0}. \tag{5}$$

The matrices of the mass, stiffness, and regular modal have the following relationship:

$$\boldsymbol{\Psi}^{\mathrm{T}}\boldsymbol{M}\boldsymbol{\Psi}=\boldsymbol{I}, \tag{6a}$$

$$\boldsymbol{\Psi}^{\mathrm{T}}\boldsymbol{C}\boldsymbol{\Psi}=\mathrm{diag}[2\zeta_s\omega_s], \tag{6b}$$

$$\boldsymbol{\Psi}^{\mathrm{T}}\boldsymbol{K}\boldsymbol{\Psi}=\mathrm{diag}[\omega_s^{2}], \tag{6c}$$

where $\boldsymbol{I}$ is the identity matrix, and ζ_s is the sth order modal damping ratio of the leaf model.

Left multiplying Eq. (1) by $\boldsymbol{\Psi}^{\mathrm{T}}$ and applying Eqs. (4) and (6a) to Eq. (6c), we can obtain

$$\ddot{\boldsymbol{\xi}}+\mathrm{diag}[2\zeta_s\omega_s]\dot{\boldsymbol{\xi}}+\mathrm{diag}[\omega_s^{2}]\boldsymbol{\xi}=\boldsymbol{\Psi}^{\mathrm{T}}\boldsymbol{f}(t)\triangleq\boldsymbol{R}(t). \tag{7}$$

Eq. (7) represents the motion differential equations of a set of a decoupled single DOF system whose frequency response function matrix is

$$\boldsymbol{H}_{\mathrm{d}}^{\xi}(\omega^{*})=\left(\mathrm{diag}[\omega_i^{2}]-(\omega^{*})^{2}\boldsymbol{I}+\mathrm{j}\,\mathrm{diag}[2\omega\zeta_i\omega_i]\right)^{-1}, \tag{8}$$

where j is the imaginary unit.

Therefore, the frequency response function matrix of the leaf model is

$$\begin{aligned}\boldsymbol{H}_{\mathrm{d}}^{x}(\omega^{*})&=\boldsymbol{\Psi}\boldsymbol{H}_{\mathrm{d}}^{\xi}(\omega^{*})\boldsymbol{\Psi}^{\mathrm{T}}\\&=\boldsymbol{\Psi}\left(\mathrm{diag}[\omega_i^{2}]-(\omega^{*})^{2}\boldsymbol{I}+\mathrm{j}\,\mathrm{diag}[2\omega^{*}\zeta_i\omega_i]\right)^{-1}\boldsymbol{\Psi}^{\mathrm{T}}\\&=\sum_{i=1}^{n}\frac{\boldsymbol{\psi}_i\boldsymbol{\psi}_i^{\mathrm{T}}}{\omega_i^{2}-(\omega^{*})^{2}+\mathrm{j}2\omega^{*}\zeta_i\omega_i}.\end{aligned} \tag{9}$$

The displacement response vector of the leaf model is

$$\begin{aligned}\boldsymbol{x}(t)&=\boldsymbol{H}_{\mathrm{d}}^{x}(\omega^{*})\boldsymbol{f}(t)\\&=\sum_{i=1}^{n}\frac{\boldsymbol{\psi}_i\boldsymbol{\psi}_i^{\mathrm{T}}}{\omega_i^2-(\omega^{*})^2+\mathrm{j}2\omega^{*}\zeta_i\omega_i}\cdot\boldsymbol{F}_{\mathrm{A}}\cos(\omega^{*}t).\end{aligned}\tag{10}$$

When the exciting force acts only on the pth DOF, the displacement response of the lth DOF is

$$\boldsymbol{x}_l^{p}(t)=\sum_{i=1}^{n}\frac{\psi_{il}\psi_{ip}}{\omega_i^2-(\omega^{*})^2+\mathrm{j}2\omega^{*}\zeta_i\omega_i}\cdot F_{\mathrm{A}}^{p}\cos(\omega^{*}t),\tag{11}$$

where ψ_{il} and ψ_{ip} are the lth and pth elements of the regular modal $\boldsymbol{\psi}_i$, respectively, and F_{A}^{p} is the amplitude of the exciting force.

The amplitude of the above displacement response of the lth DOF is

$$X_l=\sum_{i=1}^{n}\frac{\psi_{il}\psi_{ip}}{\sqrt{\left(\omega_i^2-(\omega^{*})^2\right)^2+\left(2\omega^{*}\zeta_i\omega_i\right)^2}}\cdot F_{\mathrm{A}}^{p}.\tag{12}$$

From Eq. (12), a large displacement response appears only if the excitation frequency, ω^{*}, is close to the sth order natural angular frequency, ω_s, at which $\psi_{sl}\psi_{sp}F_{\mathrm{A}}^{p}$ is larger than those at other natural angular frequencies. Structural vibration-proof design by improving lower order natural frequencies fails to include the impact of the direction of the exciting force on the structural dynamic response.

3 Stiffener layout design using an evolutionary algorithm

3.1 Growth simulation

Since the growth of leaf venation should be adaptive to random wind in the environment, its growth mechanism could probably give us inspiration for stiffener layout design for vibration-proof purposes. After observing the configurations of different types of leaf venation, we conclude that the growth of leaf venation can be considered as a process of iteratively solving the following two problems. One is about growth: finding the growth directions and calculating the geometrical dimensions of leaf veins. The other is about branching: deciding whether and how to branch. To bridge the gap between inspiration and practical application, the growth mechanism of leaf venation is analyzed from the viewpoint of mathematical and optimal design. In our FE model (Fig. 3) the leaf lamina is represented by a base plate discretized into 4-node shell elements. Each shell element is reinforced by leaf veins, referred to as stiffeners, and divided by 2-node beam elements. The eight beam elements extending from each sprouting point denote different potential growth directions for stiffeners. The cross-sections of beam elements are rectangular, their heights are constant, and their widths (t_i) are selected as variables in the growth simulation. In the initial growth stage, the stiffeners can be neglected since the widths of the beam elements are very small.

The growth model of leaf venation can be described as

$$\begin{aligned}&\text{find}\quad \boldsymbol{t}=\left[t_1,t_2,\cdots,t_N\right]^{\mathrm{T}},\\&\min\quad X_l,\\&\text{s.t.}\quad g_1(\boldsymbol{t})=W(\boldsymbol{t})-W_{\mathrm{g}}=\sum_{i=1}^{N}\rho h_{\mathrm{s}}l_it_i-W_{\mathrm{g}}\le 0,\\&\qquad 0<\boldsymbol{t}^{\mathrm{L}}\le\boldsymbol{t}\le\boldsymbol{t}^{\mathrm{U}},\end{aligned}\tag{13}$$

where $\boldsymbol{t}$ is an N-dimensional design vector; N is the total number of stiffeners to grow; t_i is the width of the ith stiffener; X_l is the growth objective function, i.e., the displacement response amplitude of the lth DOF of the leaf model; $g_1(\boldsymbol{t})$ is the constraint function; $W(\boldsymbol{t})$ is the total weight of material allocated to stiffeners at one growth step; W_{g} is the upper limit of $W(\boldsymbol{t})$; $\boldsymbol{t}^{\mathrm{L}}$ and $\boldsymbol{t}^{\mathrm{U}}$ are the lower and upper limits of $\boldsymbol{t}$, respectively; ρ is the material density of stiffeners; h_{s} and l_i are the constant height and length, respectively, of the ith stiffener.

To find the optimal solution $\boldsymbol{t}^{*}$, the Lagrange function is employed,

$$L(\boldsymbol{t},\boldsymbol{\Lambda})=X_l(\boldsymbol{t})+\boldsymbol{\Lambda}^{\mathrm{T}}\boldsymbol{g}(\boldsymbol{t})=X_l(\boldsymbol{t})+\sum_{i=1}^{3}\lambda_ig_i(\boldsymbol{t}),\tag{14}$$

where λ_i (i=1, 2, 3) are Lagrange multipliers, $\boldsymbol{\Lambda}=[\lambda_1,\lambda_2,\lambda_3]^{\mathrm{T}}$, $g_2(\boldsymbol{t})=\boldsymbol{t}^{\mathrm{L}}-\boldsymbol{t}$, $g_3(\boldsymbol{t})=\boldsymbol{t}-\boldsymbol{t}^{\mathrm{U}}$, and $\boldsymbol{g}(\boldsymbol{t})=[g_1(\boldsymbol{t}),g_2(\boldsymbol{t}),g_3(\boldsymbol{t})]^{\mathrm{T}}$.

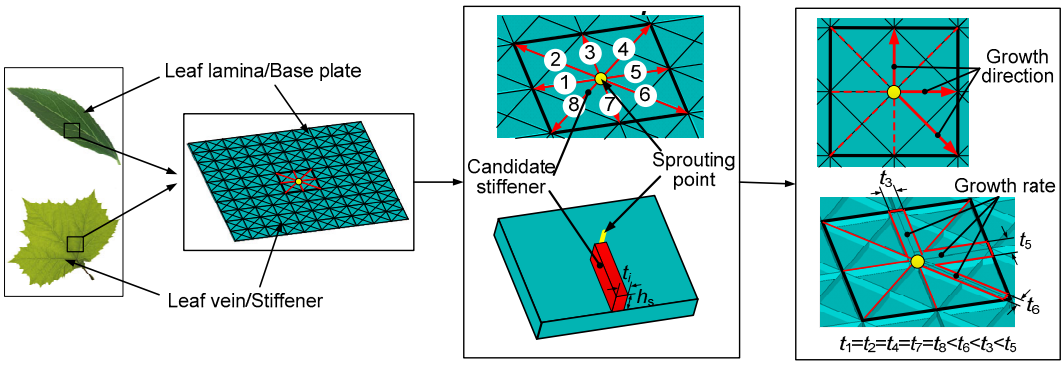

Fig. 3 FE model for growth simulation of plant leaves

According to the Kuhn-Tucker conditions, under the circumstance of optimal solution $\boldsymbol{t}^*$, the following formulas must be satisfied:

$$\begin{cases} \dfrac{\partial X_l}{\partial t_i}+\lambda_1\dfrac{\partial g_1}{\partial t_i}\begin{cases}\le 0, & t_i=t^{\mathrm{U}},\\ =0, & t^{\mathrm{L}}<t_i<t^{\mathrm{U}},\\ \ge 0, & t_i=t^{\mathrm{L}},\end{cases} & i=1,2,\cdots,N,\\ \lambda_1(W(\boldsymbol{t})-W_{\mathrm{g}})=0, \quad \begin{cases}\lambda_1=0, & W(\boldsymbol{t})<W_{\mathrm{g}},\\ \lambda_1\ge 0, & W(\boldsymbol{t})=W_{\mathrm{g}},\end{cases} \\ W(\boldsymbol{t})-W_{\mathrm{g}}\le 0,\ \boldsymbol{t}^{\mathrm{L}}\le\boldsymbol{t}\le\boldsymbol{t}^{\mathrm{U}},\\ \lambda_1\ge 0. \end{cases} \tag{15}$$

When $t^{\mathrm{L}}<t_i<t^{\mathrm{U}}$, multiplying t_i by $\dfrac{\partial X_l}{\partial t_i}+\lambda_1\dfrac{\partial g_1}{\partial t_i}$ =0 leads to

$$\lambda_1=\frac{-t_i(\partial X_l/\partial t_i)}{t_i(\partial g_1/\partial t_i)}. \tag{16}$$

The partial derivative of the constraint function is

$$\frac{\partial g_1}{\partial t_i}=\frac{\partial(W-W_{\mathrm{g}})}{\partial t_i}=\rho h_{\mathrm{s}} l_i, \quad i=1,2,\cdots,N. \tag{17}$$

Set $\bar{t}_i$ as the generalized width of the ith stiffener, which is the negative product of stiffener width and the sensitivity of the objective function with respect to the width:

$$\bar{t}_i=-t_i\frac{\partial X_l}{\partial t_i}. \tag{18}$$

Applying Eqs. (17) and (18) to Eq. (16), the Lagrange multiplier λ_1 can be expressed as

$$\begin{aligned}\lambda_1&=\frac{\bar{t}_1}{\rho h_{\mathrm{s}} l_1 t_1}=\cdots=\frac{\bar{t}_i}{\rho h_{\mathrm{s}} l_i t_i}=\cdots\\ &=\frac{\bar{t}_N}{\rho h_{\mathrm{s}} l_N t_N}=\frac{\sum_{i=1}^{N}\bar{t}_i}{\sum_{i=1}^{N}\rho h_{\mathrm{s}} l_i t_i}=\frac{\bar{t}_{\mathrm{sum}}}{W_{\mathrm{sum}}}.\end{aligned} \tag{19}$$

The width of the ith stiffener can be obtained from

$$t_i=\frac{1}{\rho h_{\mathrm{s}} l_i}\left(W_{\mathrm{sum}}\frac{\bar{t}_i}{\bar{t}_{\mathrm{sum}}}\right), \quad i=1,2,\cdots,N. \tag{20}$$

Eq. (20) shows that the width of the ith stiffener is proportional to its generalized width. Therefore, stiffeners must grow along the direction with large generalized width to optimize structural dynamic performance. The larger the generalized width, the faster the stiffener grows in that direction.

When iterating, Eq. (20) can be rewritten as

$$t_i^{(k+1)}=\left(\frac{W_{\mathrm{sum}}}{\rho h_{\mathrm{s}} l_i}\cdot\frac{\bar{t}_i}{\bar{t}_{\mathrm{sum}}}\right)^{(k)}, \quad i=1,2,\cdots,N. \tag{21}$$

3.2 Design procedure

After characterizing the optimality of leaf venation growth, an evolutionary algorithm is proposed to implement stiffener growth adaptive to the exciting force. During growth, candidate stiffeners

compete with each other for limited growth material and as a result some stiffeners grow wider than others. According to the results of this competition, the stiffener layout is gradually configured. The design flow adopting the proposed algorithm includes three basic steps: initialization, competition, and reconfiguration (Fig. 4).

3.2.1 Initialization

The growth model for stiffener layout design is built and the sprouting point set $\{B\}$ and candidate stiffener set $\{C\}$ are initialized. Meanwhile, the parameters to control stiffener growth are specified, including t_b and t_d (the threshold widths of branching and degenerating, respectively), W_g (the upper limit for the weight increment in one growth step), W_p (the weight of the base plate), and W_r (the upper limit for the total weight increment).

3.2.2 Competition

The candidate stiffeners are ready to grow and compete with each other for limited growth material (W_g). The competition strategy consists of two sub-steps, i.e., competitions for growth orientation and growth volume (Fig. 5).

Sub-step A: competition for growth orientation

1. Set the widths of all candidate stiffeners as design variables in sub-step A ($\boldsymbol{t}^1$), $\boldsymbol{t}^1=[t_1, t_2, \ldots, t_l]^{\mathrm{T}}$, and then obtain the optimal solution $\boldsymbol{t}^{1*}$ by solving the constrained extremal problem Eq. (13) according to Eq. (21).

2. Select the optimal orientation from the solution set $\boldsymbol{t}^{1*}$ based on the pre-determined threshold value (t_b). If the width of a candidate stiffener is larger than t_b, we consider it as a winner in the competition for growth orientation, and the placing direction of this stiffener is regarded as the sprouting direction for the following competition.

Sub-step B: competition for growth volume

1. Re-arrange the candidate stiffeners along the optimal growth orientation obtained in sub-step A.

2. Set the widths of the remaining stiffeners as new design variables in sub-step B ($\boldsymbol{t}^2$), $\boldsymbol{t}^2=[t_i, \ldots, t_j, \ldots, t_k]^{\mathrm{T}}$ ($i<j<k<l$), and then obtain the optimal solution $\boldsymbol{t}^{2*}$, by solving the constrained extremal problem again according to Eq. (21).

3. $\boldsymbol{t}^{2*}$ stands for the optimal material allocation in the simulation of growth competition.

3.2.3 Reconfiguration

After the growth competition, candidate stiffeners have been allocated different amounts of material. To concentrate growth material in the best growth directions, branching and degenerating operations are carried out. If the width of a candidate stiffener is no less than the threshold value for branching, t_b, the stiffener survives and will branch. Its end nodes are added to the set $\{B\}$ and the stiffeners around the new sprouting points to the set $\{C\}$. In contrast, if the stiffener width is no larger than the threshold value for degenerating, t_d, it will degenerate. Its end points and the relevant stiffeners are deleted from the sets.

Competition and reconfiguration together make up one growth step and then iterate till the final weight increment ΔW reaches the upper limit W_r. Finally, an optimal stiffener layout can be obtained.

Let $D_s=\left[(\omega_s^2-(\omega^*)^2)^2+(2\omega^*\zeta_s\omega_s)^2\right]^{-1/2}$. According to Eq. (12), the growth objective function can then be rewritten as

$$X_l=\sum_{s=1}^{n}\psi_{sl}D_s\psi_{sp}F_{\mathrm{A}}^p. \tag{22}$$

The sensitivity of the growth objective function with respect to the design variable t_i is

$$\frac{\partial X_l}{\partial t_i}=\sum_{s=1}^{n}\left(\frac{\partial\psi_{sl}}{\partial t_i}D_s\psi_{sp}+\psi_{sl}\frac{\partial D_s}{\partial t_i}\psi_{sp}+\psi_{sl}D_s\frac{\partial\psi_{sp}}{\partial t_i}\right)F_{\mathrm{A}}^p. \tag{23}$$

The derivative of D_s with respect to the ith design variable is

$$\frac{\partial D_s}{\partial t_i}=-D_s^3\left[\left(\omega_s^2-(\omega^*)^2\right)\cdot\frac{\partial(\omega_s^2)}{\partial t_i}+(2\omega^*\zeta_s\omega_s)\cdot\frac{\partial\omega_s}{\partial t_i}\right], \tag{24}$$

where

$$\frac{\partial\omega_s}{\partial t_i}=\frac{1}{2\omega_s}\cdot\frac{\partial(\omega_s^2)}{\partial t_i}. \tag{25}$$

By differentiating Eq. (5), we obtain

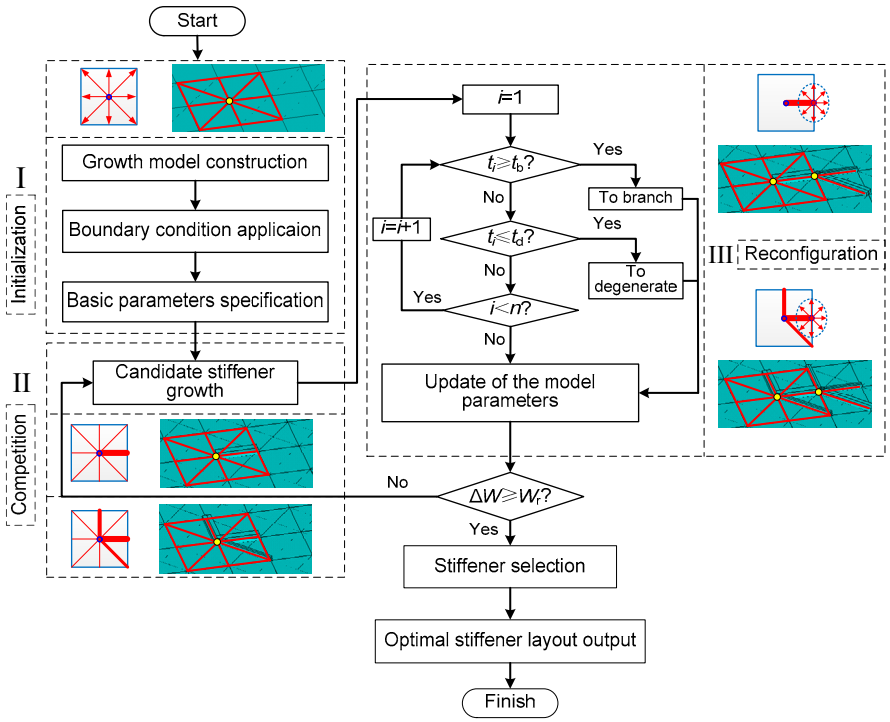

Fig. 4 Flowchart of stiffener layout design using the proposed algorithm

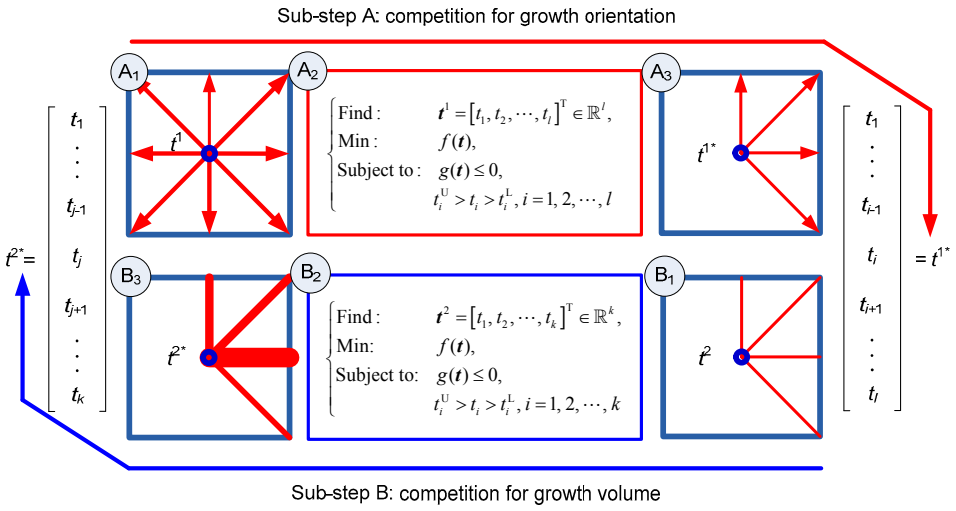

Fig. 5 Strategy for growth competition

$$\left(\frac{\partial \boldsymbol{K}}{\partial t_i}-\frac{\partial(\omega_s^2)}{\partial t_i}\boldsymbol{M}-\omega_s^2\frac{\partial \boldsymbol{M}}{\partial t_i}\right)\boldsymbol{\psi}_s+(\boldsymbol{K}-\omega_s^2\boldsymbol{M})\frac{\partial \boldsymbol{\psi}_s}{\partial t_i}=0. \tag{26}$$

Left multiplying Eq. (26) by $\boldsymbol{\psi}_s^{\mathrm{T}}$, the derivation of the square of the natural angular frequencies can be obtained:

$$\frac{\partial(\omega_s^2)}{\partial t_i}=\boldsymbol{\psi}_s^{\mathrm{T}}\left(\frac{\partial \boldsymbol{K}}{\partial t_i}-\omega_s^2\frac{\partial \boldsymbol{M}}{\partial t_i}\right)\boldsymbol{\psi}_s. \tag{27}$$

The derivative of the regular modals can be solved by employing the incomplete modal superposition solution (Alvin, 1997), in which the derivative can be expressed as the superposition of the first several regular modals.

$$\frac{\partial \boldsymbol{\psi}_s}{\partial t_i}=\sum_{k=1}^{n}\beta_{sk}\boldsymbol{\psi}_k, \tag{28}$$

where

$$\beta_{sk}=\begin{cases}\dfrac{\boldsymbol{\psi}_k^{\mathrm{T}}\left(\dfrac{\partial \boldsymbol{K}}{\partial t_i}-\omega_s^2\dfrac{\partial \boldsymbol{M}}{\partial t_i}\right)\boldsymbol{\psi}_s}{\omega_s^2-\omega_k^2}, & s\neq k,\\ -\dfrac{1}{2}\boldsymbol{\psi}_k^{\mathrm{T}}\dfrac{\partial \boldsymbol{M}}{\partial t_i}\boldsymbol{\psi}_s, & s=k,\end{cases} \tag{29}$$

where the derivatives of the stiffness matrix and mass matrix are presented in Appendix A.

4 Numerical example

A cantilever beam is chosen as the design object to validate the proposed evolutionary algorithm. The size of the cantilever beam is 120 mm×80 mm ×0.3 mm with its left end fixed (Fig. 6a). The material properties of the beam are as follows: the elastic modulus is set as 2.06×10^5 MPa, Poisson's ratio is 0.3, and the density is 7800 kg/m^3. The first two order natural frequencies of the beam are 3.60 kHz and 10.7 kHz, respectively. The first order mode of the beam is the swing in the vertical direction (Fig. 6b), and the second order mode is the telescopic movement in the horizontal direction (Fig. 6c). The stiffener layout design is conducted with the proposed algorithm with a harmonic force applied to the middle point of the right end of the beam. Six cases are studied with the exciting force at frequencies of 0, 1500, and 3000 Hz, applied along the horizontal (x) and vertical (y) directions.

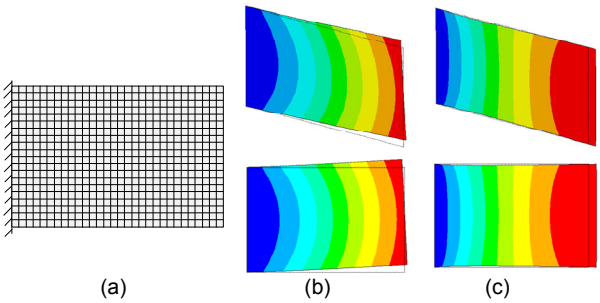

Fig. 6 Simulated cantilever beam: (a) mesh of the cantilever beam; (b) first order mode; (c) second order mode

4.1 Stiffener layout design under vertical excitation

A harmonic force, $f(t)=\cos(2\pi ft)$ N, is applied along the vertical direction. The height of the candidate stiffeners is set as 0.9 mm. The initial width of stiffeners and the threshold value for degenerating, t_d, are 0.001 mm and the threshold value for branching, t_b, is 6 mm. The upper limit for material consumption by stiffeners, W_r, is 1.2 times the weight of the initial cantilever beam, W_p. Fig. 7 shows the growth processes of stiffeners under harmonic force at different frequencies in the vertical direction, the first order natural frequencies of the beams during the growth process, and the displacement amplitude of the force acting point.

Since the movement of the cantilever beam is along the vertical direction in its first order mode, a vertical exciting force has the potential to cause resonance as its frequency approaches the beam's first order natural frequency. Therefore, as the excitation frequency increases from 0 Hz to 3000 Hz, more growth material is allocated close to the fixed side of the beam to improve the corresponding natural frequency.

The changes in the amplitude of the displacement response of the initial and optimized cantilever beams with excitation frequency are shown in Fig. 8. Compared with the initial cantilever beam, the displacement response amplitude of the optimized beams is clearly reduced. In addition, all optimized beams effectively avoid the appearance of resonance under their corresponding exciting forces. The effectiveness of the proposed method is thus proved.

4.2 Stiffener layout design under horizontal excitation

The same harmonic force is applied in the horizontal direction, and the parameters controlling the growth of stiffeners are the same as those in Section 4.1. The growth processes of the stiffeners are shown in Fig. 9 (p.943).

The stiffener growth processes under horizontal harmonic forces with different frequencies are almost the same. The relative difference in the second order natural frequencies among the optimized beams is very small. The main reason for this similarity is that the frequencies of the exciting forces are

Excitation frequency (kHz) \ Material consumption		$0.3W_p$	$0.6W_p$	$0.9W_p$	$1.2W_p$
0	Adaptive grow process	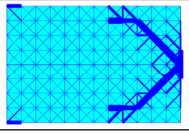	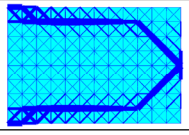	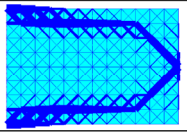	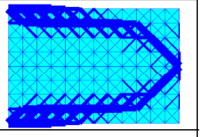
	First order natural frequency	3541.1 Hz	3544.2 Hz	3807.1 Hz	3841.5 Hz
	Displacement amplitude	2.73×10^{-4} mm	1.78×10^{-4} mm	1.44×10^{-4} mm	1.26×10^{-4} mm
1.5	Adaptive grow process	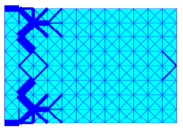	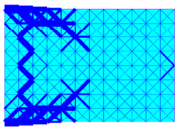	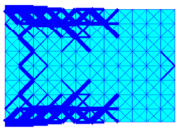	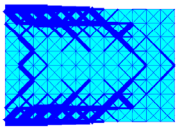
	First order natural frequency	4098.2 Hz	4227.7 Hz	4336.5 Hz	4353.8 Hz
	Displacement amplitude	2.92×10^{-4} mm	1.83×10^{-4} mm	1.62×10^{-4} mm	1.35×10^{-4} mm
3.0	Adaptive grow process	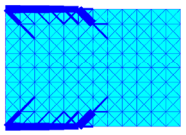	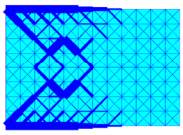	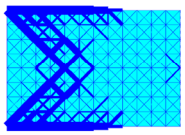	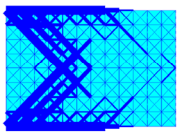
	First order natural frequency	4563.1 Hz	4815.5 Hz	4898.4 Hz	4933.6 Hz
	Displacement amplitude	3.26×10^{-4} mm	2.22×10^{-4} mm	1.84×10^{-4} mm	1.64×10^{-4} mm

Fig. 7 Stiffener growth processes under a vertical harmonic force

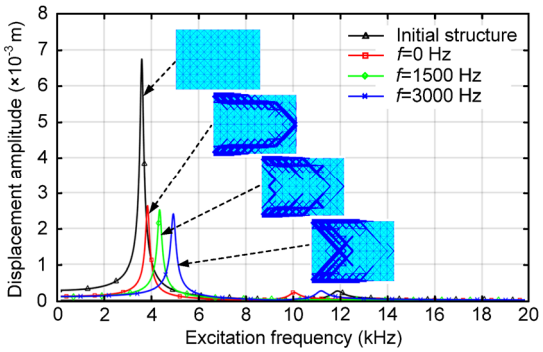

Fig. 8 Comparison of displacement amplitudes of the initial and optimized structures

far lower than the second order natural frequency of the initial cantilever beam. The exciting forces could hardly cause resonance even if they are applied in the horizontal direction, the same direction as the motion in the beam's second order mode.

The changes in the amplitude of the displacement response of the initial and optimized cantilever beams with excitation frequency are shown in Fig. 10. Similar to the design examples under vertical excitation, the displacement response amplitude of optimized beams in resonance is reduced due to the support of stiffeners. But the increases in the second order natural frequencies of the optimized beams are not as great as those under vertical excitation, as a result of there being less need to avoid excitation frequencies.

5 Conclusions

In this study, we considered the stiffener layout design problem of stiffened plate/shell structures subjected to a harmonic exciting force. By using the adaptive growth mechanism of leaf venation, an evolutionary algorithm was proposed with the objective to minimize the displacement response amplitude at specified locations. Based on the results presented in this paper, the following conclusions can be drawn:

1. Both the direction and frequency of the exciting force influence the structural displacement response. Therefore, both factors should be considered in stiffener layout design for vibration-proof purposes.

Excitation frequency (kHz) \ Material consumption		$0.3W_p$	$0.6W_p$	$0.9W_p$	$1.2W_p$
0	Adaptive grow process	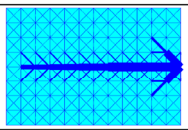	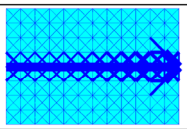	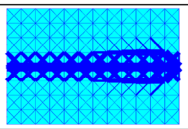	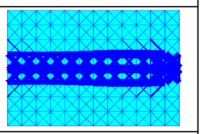
	Second order natural frequency	9892.5 Hz	10 021.2 Hz	10 097.4 Hz	10 929.5 Hz
	Displacement amplitude	2.87×10^{-5} mm	2.54×10^{-5} mm	2.27×10^{-5} mm	1.79×10^{-5} mm
1.5	Adaptive grow process	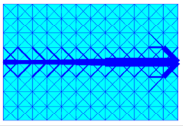	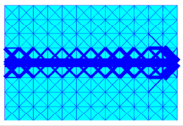	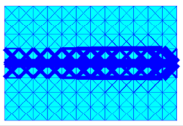	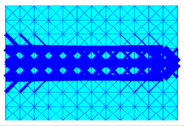
	Second order natural frequency	9979.3 Hz	10 249.4 Hz	10 786.4 Hz	11 323.0 Hz
	Displacement amplitude	2.99×10^{-5} mm	2.64×10^{-5} mm	2.33×10^{-5} mm	1.89×10^{-5} mm
3.0	Adaptive grow process	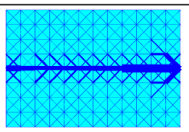	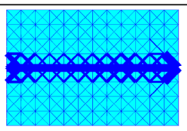	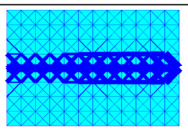	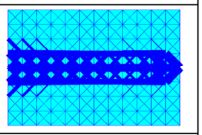
	Second order natural frequency	10 132.1 Hz	10 352.6 Hz	11 015.2 Hz	11 402.1 Hz
	Displacement amplitude	3.18×10^{-5} mm	2.85×10^{-5} mm	2.50×10^{-5} mm	2.01×10^{-5} mm

Fig. 9 Stiffener growth processes under a horizontal harmonic force

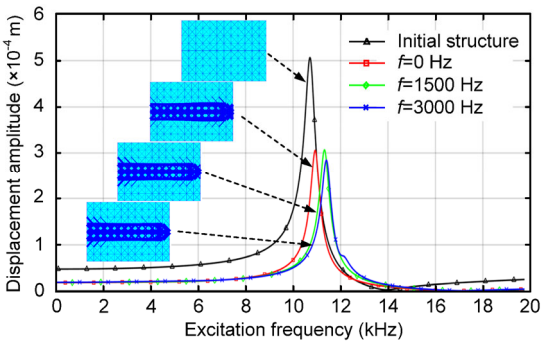

Fig. 10 Comparison of displacement amplitudes of the initial and optimized structures

2. The growth of leaf venation was analyzed from the perspective of optimization, and the equation governing the growth process was drawn, which showed that the growth of leaf veins/stiffeners is controlled by a group of variables termed generalized widths.

3. In designing a cantilever beam under harmonic excitation with the proposed approach, the growth of stiffeners shows great adaptiveness to the exciting force in terms of the direction and frequency of excitation, as expected. All the optimized cantilever beams showed an obvious improvement in dynamic performance. Therefore, the proposed approach has the potential to facilitate vibration-proof design of stiffened plate/shell structures. Although the optimized beams have complex layouts, they could be conveniently manufactured using additive manufacturing technologies.

Future work will involve further development of the proposed approach by taking chatter reliability into consideration and by application to the design of structures under more complex excitation.

References

Alvin, K., 1997. Efficient computation of eigenvector sensitivities for structural dynamics. *AIAA Journal*, **35**(11): 1760-1766. http://dx.doi.org/10.2514/3.13742

Benz, M., Kovalev, A., Gorb, S., 2012. Anisotropic frictional properties in snakes. Proceedings of SPIE 8339, Bioinspiration, Biomimetics, and Bioreplication, CA, USA, p.1-6. http://dx.doi.org/10.1117/12.916972

Bhogal, S.S., Sindhu, C., Dhami, S.S., *et al.*, 2015. Minimization of surface roughness and tool vibration in CNC

milling operation. *Journal of Optimization*, **2015**:192030. http://dx.doi.org/10.1155/2015/192030

Campa, F.J., Lopez de Lacalle, L.N., Celaya, A., 2011. Chatter avoidance in the milling of thin floors with bull-nose end mills: model and stability diagrams. *International Journal of Machine Tools and Manufacture*, **51**(1):43-53. http://dx.doi.org/10.1016/j.ijmachtools.2010.09.008

Díaz-Tena, E., Rodríguez-Ezquerro, A., López de Lacalle Marcaide, L.N., *et al.*, 2014. A sustainable process for material removal on pure copper by use of extremophile bacteria. *Journal of Cleaner Production*, **84**:752-760. http://dx.doi.org/10.1016/j.jclepro.2014.01.061

Ding, X., Yamazaki, K., 2004. Stiffener layout design for plate structures by growing and branching tree model (application to vibration-proof design). *Structural and Multidisciplinary Optimization*, **26**(1-2):99-110. http://dx.doi.org/10.1007/s00158-003-0309-4

Gaul, L., Becker, J., 2014. Reduction of structural vibrations by passive and semiactively controlled friction dampers. *Shock and Vibration*, **2014**:870564. http://dx.doi.org/10.1155/2014/870564

Graham, E., Mehrpouya, M., Park, S.S., 2013. Robust prediction of chatter stability in milling based on the analytical chatter stability. *Journal of Manufacturing Processes*, **15**(4):508-517. http://dx.doi.org/10.1016/j.jmapro.2013.08.005

Haber, R., Bendsoe, M., Jog, C., 1996. A new approach to variable-topology shape design using a constraint on the perimeter. *Structural Optimization*, **11**:1-12. http://dx.doi.org/10.1007/BF01279647

Herranz, S., Campa, F.J., Lopez de Lacalle, L.N., *et al.*, 2005. The milling of airframe components with low rigidity: a general approach to avoid static and dynamic problems. *Proceedings of the Institution of Mechanical Engineers, Part B: Journal of Engineering Manufacture*, **219**(11): 789-801. http://dx.doi.org/10.1243/095440505X32742

Li, B., Hong, J., Wang, Z., *et al.*, 2013a. An innovative layout design methodology for stiffened plate/shell structures by material increasing criterion. *Journal of Engineering Materials and Technology*, **135**(2):1-11. http://dx.doi.org/10.1115/1.4023781

Li, B., Hong, J., Yan, S., *et al.*, 2013b. Multidiscipline topology optimization of stiffened plate/shell structures inspired by growth mechanisms of leaf veins in nature. *Mathematical Problems in Engineering*, **2013**:653895. http://dx.doi.org/10.1155/2013/653895

Li, F., Liu, W., Fu, X., *et al.*, 2012. Jumping like an insect: design and dynamic optimization of a jumping minirobot based on bio-mimetic inspiration. *Mechatronics*, **22**(2): 167-176. http://dx.doi.org/10.1016/j.mechatronics.2012.01.001

Li, G., Wang, W., Li, H., 2013. Experiment and application of market-based control for engineering structures. *Journal of Applied Mathematics*, **2013**:219537. http://dx.doi.org/10.1155/2013/219537

Li, X., Shen, Y., Wang, S., 2011. Dynamic modeling and analysis of the large-scale rotary machine with multi-supporting. *Shock and Vibration*, **18**(1-2):53-62. http://dx.doi.org/10.1155/2011/541049

Liu, H., Zhang, W., Zhu, J., 2013. Structural topology optimization and frequency influence analysis under harmonic force excitations. *Chinese Journal of Theoretical and Applied Mechanics*, **45**(4):588-597. http://dx.doi.org/10.6052/0459-1879-12-253

Liu, H., Zhang, W., Gao, T., 2015. A comparative study of dynamic analysis methods for structural topology optimization under harmonic force excitations. *Structural and Multidisciplinary Optimization*, **51**(6):1321-1333. http://dx.doi.org/10.1007/s00158-014-1218-4

Liu, W., Gong, J., Liu, X., *et al.*, 2009. A kind of innovative design methodology of wind turbine blade based on natural structure. Second International Conference on Information and Computing Science, Manchester, UK, **4**:350-354. http://dx.doi.org/10.1109/icic.2009.399

Liu, Y., Li, T.X., Liu, K., *et al.*, 2016. Chatter reliability prediction of turning process system with uncertainties. *Mechanical Systems and Signal Processing*, **66-67**:232-247. http://dx.doi.org/10.1016/j.ymssp.2015.06.030

Meehan, P.A., 2002. Vibration instability in rolling mills: modeling and experimental results. *Journal of Vibration and Acoustics*, **124**(2):221-228. http://dx.doi.org/10.1115/1.1456457

Palmer, J., Paez, T., 2011. Dynamic response of an optomechanical system to a stationary random excitation in the time domain. *Shock and Vibration*, **18**(5):747-758. http://dx.doi.org/10.1155/2011/607923

Rashid, A., Ramli, R., Haris, S., *et al.*, 2014. Improving the dynamic characteristics of body-in-white structure using structural optimization. *The Scientific World Journal*, **2014**:1-11. http://dx.doi.org/10.1155/2014/190214

Senba, A., Oka, K., Takahama, M., *et al.*, 2013. Vibration reduction by natural frequency optimization for manipulation of a variable geometry truss. *Structural and Multidisciplinary Optimization*, **48**(5):939-954. http://dx.doi.org/10.1007/s00158-013-0933-6

Tsai, T., Cheng, C., 2013. Structural design for desired eigenfrequencies and mode shapes using topology optimization. *Structural and Multidisciplinary Optimization*, **47**(5):673-686. http://dx.doi.org/10.1007/s00158-012-0840-2

Viadero, F., Bueno, J.I., Lopez de Lacalle, L.N., *et al.*, 1994. Reliability computation on stiffened bending plates. *Advances in Engineering Software*, **20**(1):43-48. http://dx.doi.org/10.1016/0965-9978(94)90029-9

Wetherhold, R., Padliya, P.S., 2014. Design aspects of nonlinear vibration analysis of rectangular orthotropic membranes. *Journal of Vibration and Acoustics*, **136**(3): 034506. http://dx.doi.org/10.1115/1.4027148

Whalley, R., Abdul-Ameer, A.A., Ebrahimi, K.M., 2011. The axes response and resonance identification for a machine

tool. *Mechanism and Machine Theory*, **46**(8):1171-1192. http://dx.doi.org/10.1016/j.mechmachtheory.2011.02.012

Zhang, Z., Karimi, H., Huang, H., *et al.*, 2014. Vibration control of a semiactive vehicle suspension system based on extended state observer techniques. *Journal of Applied Mathematics*, **2014**:248297. http://dx.doi.org/10.1155/2014/248297

Zhou, M., Rozvany, G., 1991. The COC algorithm, part II: topological, geometry and generalized shape optimization. *Computer Methods in Applied Mechanics and Engineering*, **89**:309-336. http://dx.doi.org/10.1016/0045-7825(91)90046-9

中文概要

题　目： 简谐力激励下结构的生长式拓扑优化方法

目　的： 振动在机械结构的工作中难以避免，且会显著降低机械结构的工作性能。因此，结构动力响应优化设计就显得尤为重要。本文旨在提出一种有效的简谐力激励下的结构拓扑优化方法，通过合理设计结构内加强筋的布局，减小结构特定位置处的位移响应幅值，提高结构的固有频率。

概　要： 植物叶脉可以有效地支撑叶片以抵抗自然界中的风载。本文将植物叶脉分叉构型的最优性用于简谐力激励下结构的加强筋布局设计。首先对简谐力激励下结构的位移响应进行分析。在此基础上，构建以最小化结构特定位置处位移响应幅值为目标的生长式拓扑优化模型。然后，从数学优化的角度，分析加强筋的生长应遵循的规律，提出生长式拓扑优化的数值实现算法。最后通过数值算例证明了本文所提方法的有效性。

关键词： 拓扑优化；适应性生长；刚度设计；加强筋布局；简谐力激励

Appendix A

To calculate the sensitivity of the growth objective function, the derivatives of the stiffness matrix and mass matrix of the jth candidate stiffener with respect to the ith design variable are needed. When $j\neq i$, the derivatives of the matrices are zero. When $j=i$, the derivatives are as follows:

$$\frac{\partial \boldsymbol{K}_j}{\partial t_i}=\begin{bmatrix}
\frac{Eh}{l_j} & & & & & & & & & & & \\
0 & \frac{Eh^3}{l_j^3} & & & & & & & & & & \\
0 & 0 & \frac{3Et_i^2h}{l_j^3} & & & & & & & & & \\
0 & 0 & 0 & \frac{Gh^3+3Gt_i^2h}{12l_j} & & & & & & & & \\
0 & 0 & \frac{-3Et_i^2h}{2l_j^2} & 0 & \frac{3Et_i^2h}{3l_j} & & & & & & & \\
0 & \frac{Eh^3}{2l_j^2} & 0 & 0 & 0 & \frac{Eh^3}{3l_j} & & & & & & \\
-\frac{Eh}{l_j} & 0 & 0 & 0 & 0 & 0 & \frac{Eh}{l_j} & & & & & \\
0 & \frac{-Eh^3}{l_j^3} & 0 & 0 & 0 & -\frac{Eh^3}{2l_j^2} & 0 & \frac{Eh^3}{l_j^3} & & & & \\
0 & 0 & \frac{-3Et_i^2h}{l_j^3} & 0 & \frac{3Et_i^2h}{2l_j^2} & 0 & 0 & 0 & \frac{3Et_i^2h}{l_j^3} & & & \\
0 & 0 & 0 & -\frac{Gh^3+3Gt_i^2h}{12l_j} & 0 & 0 & 0 & 0 & 0 & \frac{Gh^3+3Gt_i^2h}{12l_j} & & \\
0 & 0 & \frac{-3Et_i^2h}{2l_j^2} & 0 & \frac{Et_i^2h}{2l_j} & 0 & 0 & 0 & \frac{3Et_i^2h}{2l_j^2} & 0 & \frac{Et_i^3}{3l_j} & \\
0 & \frac{Eh^3}{2l_j^2} & 0 & 0 & 0 & \frac{Eh^3}{6l_j} & 0 & \frac{-Eh^3}{6l_j^2} & 0 & 0 & 0 & \frac{Eh^3}{3l_j}
\end{bmatrix}, \quad \text{(A1)}$$

(symmetric)

$$\frac{\partial \boldsymbol{M}_j}{\partial t_i}=\begin{bmatrix}
\frac{\rho l_j h}{3} & & & & & & \frac{\rho l_j h}{6} & & & & & \\
& \frac{13\rho l_j h}{35} & & & & \frac{11\rho l_j^2 h}{210} & & \frac{9\rho l_j h}{70} & & & & -\frac{13\rho l_j^2 h}{420} \\
& & \frac{13\rho l_j h}{35} & & -\frac{11\rho l_j^2 h}{210} & & & & \frac{9\rho l_j h}{70} & & \frac{13\rho l_j^2 h}{420} & \\
& & & \frac{\rho l_j h^3+3\rho l_j t_i^2 h^3}{36} & & & & & & \frac{\rho l_j h^3+3\rho l_j t_i^2 h^3}{72} & & \\
& & -\frac{11\rho l_j^2 h}{210} & & \frac{\rho l_j^3 h}{105} & & & & -\frac{13\rho l_j^2 h}{420} & & -\frac{\rho l_j^3 h}{140} & \\
& \frac{11\rho l_j^2 h}{210} & & & & \frac{\rho l_j^3 h}{105} & & \frac{13\rho l_j^2 h}{420} & & & & -\frac{\rho l_j^3 h}{140} \\
\frac{\rho l_j h}{6} & & & & & & \frac{\rho l_j h}{3} & & & & & \\
& \frac{9\rho l_j h}{70} & & & & \frac{13\rho l_j^2 h}{420} & & \frac{13\rho l_j h}{35} & & & & -\frac{11\rho l_j^2 h}{210} \\
& & \frac{9\rho l_j h}{70} & & -\frac{13\rho l_j^2 h}{420} & & & & \frac{13\rho l_j h}{35} & & \frac{11\rho l_j^2 h}{210} & \\
& & & \frac{\rho l_j h_i^3+3\rho l_j t_i^2 h^2}{72} & & & & & & \frac{\rho l_j h^3+3\rho l b_i^2 h^3}{36} & & \\
& & \frac{13\rho l_j^2 h}{420} & & -\frac{\rho l_j^3 h}{140} & & & & \frac{11\rho l_j^2 h}{210} & & \frac{\rho l_j^3 h}{105} & \\
& -\frac{13\rho l_j^2 h}{420} & & & & -\frac{\rho l_j^3 h}{140} & & -\frac{11\rho l_j^2 h}{210} & & & & \frac{\rho l_j^3 h}{105}
\end{bmatrix}. \quad \text{(A2)}$$